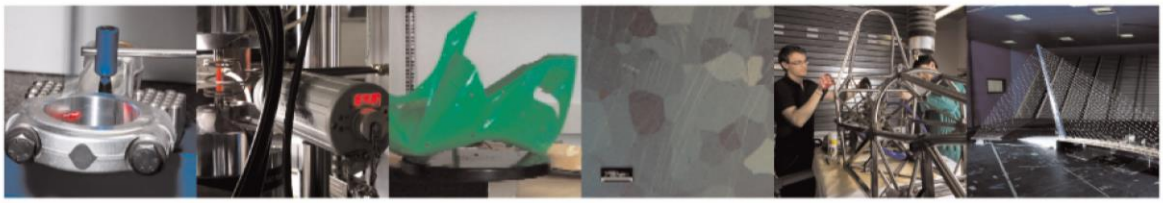

A variational model for 3D tolerance analysis with manufacturing signature and operating conditions

Corrado, A.; Polini, W.; Moroni, G.; Petro, S.

This is a post-peer-review, pre-copyedit version of an article published in Corrado, A., Polini, W., Moroni, G. and Petrò, S. (2018), "A variational model for 3D tolerance analysis with manufacturing signature and operating conditions", Assembly Automation, Vol. 38 No. 1, pp. 10-19. The final authenticated version is available online at: http://dx.doi.org/10.1108/AA-01-2017-006

DIPARTIMENTO DI MECCANICA ■ POLITECNICO DI MILANO
via G. La Masa, 1 ■ 20156 Milano ■ EMAIL (PEC): pecmecc@cert.polimi.it
http://www.mecc.polimi.it
Rev. 0

A variational model for 3D Tolerance Analysis with manufacturing signature and operating conditions

Andrea Corrado[a], Wilma Polini[a,*], Giovanni Moroni[b] , Stefano Petrò[b]

[a]Department of Civil and Mechanical Engineering, Università di Cassino e del Lazio Meridionale, via G. di Biasio 43, 03043 Cassino, Italy

[b]Depatment of Mechanical Engineering, Politecnico di Milano, via La Masa 1, 20156 Milano, Italy

* Corresponding author. Tel.: +39-0776-2993679; fax: +39-0776-2993546. *E-mail address:* polini@unicas.it

A variational model for 3D Tolerance Analysis with manufacturing signature and operating conditions

Abstract

Purpose of this paper	The variational model is one of the methods proposed in literature for tolerance analysis but it cannot deal with form tolerances and assembly conditions that may influence the functional requirements of mechanical assemblies.
Design/methodology/approach	This work shows how to manage the actual surfaces generated by the manufacturing process and the operating conditions inside the variational model that has been modified to integrate the manufacturing signature left on the surfaces of the parts and the operating conditions that arise during an actual assembly, such as gravity and friction. Moreover, a geometrical model was developed to numerically simulate what happens in a real assembly process and to give a reference value.
Findings	The new variational model was applied to a 3D case study. The obtained results were compared to those due to the geometrical model and to those of the variational model to validate the new model and to show the improvements.
Research limitations/implications	The proposed approach may be extended to other models of literature. Its limit is that it is able to deal with a sphere-plane contact.

Practical implications	Tolerance analysis is a valid tool to foresee geometric interferences among the components of an assembly before getting the physical assembly. It involves a decrease of the manufacturing costs.
Social implications	
What is original/value of paper	The main contributions are the insertion of a systematic pattern characterizing the features manufactured by a process, the assembly operating conditions, and the development of a geometrical model to reproduce what happens in a real assembly process.

Keywords: 3D tolerance analysis, manufacturing signature, friction, gravity

1. Introduction

Tolerance analysis supports design and manufacturing of any product. To standardize the products and the proper functioning of the assembly, it is important to assign dimensional and geometric tolerances to assembly components. Lower costs per assembly and higher probability of fit result by a right allocation of tolerances among the different parts of an assembly, since the number of rejected parts and the amount of rework required on components is reduced.

Following an assembly sequence, dimensions and tolerances of assembly components combine, to generate the tolerance stack-up functions. To solve a tolerance stack-up function means to combine the nominal values and the tolerance ranges assigned to the single assembly components in order to obtain the average value and the tolerance range of a product function. Literature presents many approaches for tolerance analysis of rigid assemblies (Chen et al., 2014, Polini, 2011), but they neglect form deviations, since they reduce geometric deviations to translational and rotational part feature defects (Ameta et al., 2011, Bo et al., 2013, Polini, 2012). Moreover, none of them is so general to be univocally accepted.

Further papers take into account form deviations, such as Samper et al. modelled form deviations of planar features by a modal description that depends on the approximation of form deviations by eigen-shapes (Samper et al., 2009). This approximation is overcome with the approaches of (Paetzold et al., 2007, Stoll et al., 2010), which are based on surface registration techniques.

All these methods cannot simulate the assembly behaviour of variant parts based on their point cloud representation, but point clouds are commonly obtained by manufacturing and measurement applications. Therefore, to have CAT tools that deal with point clouds is highly desirable to connect design, manufacturing and inspection. A skin model framework has been developed for the tolerance analysis (Anwer et al., 2014, Schleich et al., 2014), based on a representation of non-ideal workpieces that employ point clouds. Another work uses Legendre-Fourier polynomials to model cylindricity error into a Jacobian-Torsor model for tolerance analysis (Weihua and Zhenqiang, 2013).

In a previous work, the authors developed a geometric approach to take into account form deviation, together with those due to location and orientation, satisfying the Geometric Product Specification standards (Moroni and Polini, 2003).

The present paper shows two approaches to introduce point cloud schemes in a computer-aided tolerance analysis of rigid assemblies. The main contributions to the state of the art are two. The first can be found in the idea of inserting a point cloud scheme, representing a systematic pattern characterizing all the features manufactured by a process, and the assembly operating conditions, such as gravity and friction, inside a model for 3D tolerance analysis. It extends the preliminary considerations reported in (Corrado et al., 2016), by considering all the assembly conditions of the reference case study. A larger series of applications strengthen the effectiveness of the proposed model.

The second main contribution is the development of a geometrical model, reproducing what happens in a real assembly process, in order to have a reference to validate the proposed approach.

The considered 3D model for tolerance analysis is a variational one; this model was introduced and developed in (Boyer and Stewart, 1991, Gupta and Turner, 1993, Martino and Gabriele, 1989). It uses a parametric mathematical model to represent the variability of an assembly, due to tolerances and

assembly constraints. It takes ideal surfaces into account, so the contact points among profiles belonging to coupled parts are generally considered uncorrelated.

Moreover, there is a growing interest in considering working conditions and operating windows in CAT (Anselmetti et al., 2010, Armillotta and Semeraro, 2013), so the variational model was modified to take the point cloud representation of the components, into account, the friction, and the gravity that occur during assembly. The new variational model was applied to a 3D case study, by investigating all the possible assembly conditions. To validate the proposed variational model, a pure geometrical model was used as reference tool for comparison. Then, the obtained results were compared to the results from a pure variational model without signature in order to show the improvement over the state of the art.

The paper is organized as follow: in Sec. 2, how the new variational model adopts a point cloud logic in order to represent form deviation is shown. In Sec. 3, the operating conditions of assembly are introduced in the new variational model. In Sec. 4, a numerical validation by using a geometrical simulation model is presented in detail. Finally, in Sec. 5, the results are compared and discussed.

2. A point cloud variational model

This work starts by the variational model in (Marziale and Polini, 2010). The case study of this work is made up an assembly of three parts, as shown in Figure 1, in order to explain the new model. The assembly is constituted by a hollow box, that is considered nominal, and two spheres, that are affected by a dimensional and a geometrical tolerances. The target is the gap *g* between the upper sphere and the top side of the box; it depends on the tolerances applied to each component.

The point cloud representation of each sphere is a set of 235,822 evenly distributed points i.e. the points are angularly separated by 0.45°. The size of the set is adequate to accurately simulate the assembling process without slowing down the simulation excessively. Each point of the sphere has the following error model:

$$\left|\mathbf{P}_i - \mathbf{O}\right| = R + r + d \tag{1}$$

where $\mathbf{P}_i$ is a generic point of the circular profile, $\mathbf{O}$ is the centre of the circle, R is the nominal value of the radius of the sphere (equal to 20 mm), r is the average deviation from the nominal radius due to the

dimensional tolerance (equal to ± 0.0145 mm) of each sphere, and *d* is the deviation due to the manufacturing signature that should remain inside the form tolerance (equal to 0.0145 mm) applied to the spheres.

The *r* parameter has a Gaussian density function with mean value equal to zero and standard deviation equal to one sixth of the dimensional tolerance range.

A Simultaneous Autoregressive Model SAR (Cressie, 2015) represents the manufacturing signature left on the sphere by the process. This model allows to simulate phenomena that are spatially correlated in more than one dimension, whereas traditional time series models, like the ARMAX model adopted in the 2D case (Ascione et al., 2010), can represent correlation along a single direction only. It models the spatial structure of the lattice defined by the triangulation of the points on the surface of the sphere at their nominal coordinates to generate a spatially correlated set of deviations from the perfect sphericity. The first order model SAR(1) was considered, since it is simple and suitable to simulate deviations on a finite number of points.

SAR(1) model simulates the deviations from perfect sphericity **d** as :

$$\mathbf{d} = \left(\mathbf{I} - \mathbf{G}\right)^{-1} \boldsymbol{\varepsilon} \tag{2}$$

d is a vector containing the deviations (one element per point), **I** is the identity matrix and $\boldsymbol{\varepsilon} \sim N\left(\mathbf{0}, \sigma^2 \mathbf{I}\right)$ is a white noise, whose σ is equal to 0.0024 mm, and $\mathbf{G} = \rho \mathbf{W}$. ρ is a correlation coefficient: higher values of ρ denote a higher degree of spatial correlation among nearby points. In this paper, its value is set equal to 0.9. $\mathbf{W}$ is a neighbourhood matrix defined on the triangulation of the points on the surface of the sphere, whose elements

$$w_{ij} = \frac{\frac{I_{ij}}{D_{ij}}}{\sum_k \frac{I_{kj}}{D_{kj}}} \tag{3}$$

in which D_{ij} is the Cartesian distance between the $\mathbf{P}_i$ and the $\mathbf{P}_j$ points of the sphere, and I_{ij} is an indicator variable, which denotes whether points *i* and *j* are neighbours, that is

$$I_{ij} = \begin{cases} 1, \text{if point } i \text{ and } j \text{ belong to a same triangle} \\ 0, \text{otherwise} \end{cases} \quad (4)$$

An example of a sphere having deviations simulated according to (4) is shown in Figure 2.

Three configurations of the two spheres have been simulated, as shown in Figure 3, that are all the possible arrangements to insert randomly two spheres in the box. Configurations 1 and 3 consider the spheres in contact with one of the sides of the box, as shown in Figure 4 and Figure 6; considerations valid for configuration 1 are valid for configuration 3 as well. Differently, in configuration 2 the spheres are aligned along one of the four diagonals of the box, as shown in Figure 5.

The new variational model is shown in Figure 7. The first step simulates two spheres by means of eq. (1) to obtain two clouds of 235,822 points, whose centre of gravity has been calculated by the arithmetic mean of all the points coordinates. A datum reference frame (DRF) X_i-Y_i-Z_i with i=1...8 has been assigned to each surface of the box and to the centres of gravity of the two clouds (see Figure 8), while an absolute X-Y-Z reference system has been placed at the intersection among the left, the back and the bottom sides of the box, as shown in Figure 8.

Figure 9 shows an assembly graph with three spherical slider joints between the box and the first sphere SPH_1 at points A, B and C, one spherical joint between sphere SPH_1 and sphere SPH_2 at point D, two spherical slider joints between sphere SPH_2 and the box at points F and E, and the gap to estimate *g* (Corrado et al., 2016).

The equations of the geometric features in the global DRF of the assembly are evaluated by means of the following equations:

$$\mathbf{S_1}: -r_{z_{01}} X + Y + r_{x_{01}} Z + \left(25r_{z_{01}} - 25r_{x_{01}} - t_{y_{01}}\right) = 0 \quad (5)$$

$$\mathbf{S_2}: -X - r_{z_{02}} Y + r_{x_{02}} Z + \left(40r_{z_{02}} - 25r_{x_{02}} + \left(50 - t_{y_{02}}\right)\right) = 0 \quad (6)$$

$$\mathbf{S_3}: r_{z_{03}} X - Y + r_{x_{03}} Z + \left(-25r_{z_{03}} - 25r_{x_{03}} + \left(80 - t_{y_{01}}\right)\right) = 0 \quad (7)$$

$$\mathbf{S_4}: X + r_{z04} Y + r_{x04} Z + \left(-25r_{x_{04}} - 40r_{z_{04}} - t_{y04}\right) = 0 \quad (8)$$

$$\mathbf{S_5}: -r_{z05} X - r_{x05} Y + Z + \left(40r_{x_{05}} + 25r_{z_{05}} - t_{y05}\right) = 0 \quad (9)$$

$$\mathbf{S_6}: -r_{z06}X + r_{x06}Y - Z + \left(25r_{x_{06}} - 40r_{z_{06}} + 50 - t_{y06}\right) = 0 \quad (10)$$

$$\mathbf{SPH_1}: \left(X - \Delta X_{12} - O_{12X}\right)^2 + \left(Y - \Delta Y_{12} - O_{12Y}\right)^2 = \left(R_1 + r_1 + d_1\right)^2 \quad (11)$$

$$\mathbf{SPH_2}: \left(X - \Delta X_{13} - O_{13X}\right)^2 + \left(Y - \Delta Y_{13} - O_{13Y}\right)^2 = \left(R_2 + r_2 + d_2\right)^2 \quad (12)$$

where r_{x_i} and r_{z_i} are the rotation parameters of the generic feature S_i around the x and z axes of their DRF in Figure 8, t_{y_i} is the translation parameter of the generic feature S_i along y-axis of its DRF, r_1 and r_2 are the model parameter, due to the dimensional tolerances, applied to the first and the second sphere respectively, d_1 and d_2 are the model parameters, due to the form tolerance, applied to the first and the second sphere respectively, ΔX_{12}, ΔY_{12} and ΔZ_{12} are the assembly parameters of the first sphere, ΔX_{13}, ΔY_{13} and ΔZ_{13} are the assembly parameters of the second sphere in the box. The parameters r_{x_i}, r_{z_i} and t_{y_i} of the features of the box are equal to zero, since the box has been considered free of any dimensional or geometric deviation.

According with the assembly graph, the functional requirement g must be measured between the feature S_3 of the box and the G point of the second sphere SPH_2. The equation of S_3 in the global DRF of the assembly is known by eq. (7), and the equation of SPH_2 in the global DRF of the assembly is known by eq. (12), but its assembly parameters are unknown. Therefore, to determine the assembly parameters, firstly studying the assembly between the box and the first sphere is necessary , and then the assembly between the obtained sub-assembly and the second sphere.

Three spherical slider constrains allow the assembly of the sphere SPH_1 with the features S_1, S_4 and S_5 of the box:

$$\mathbf{SPH_1\text{-}S_1}: -r_{z01}\left(\Delta X_{12} + 20\right) + \left(\Delta Y_{12} + 20\right) + r_{x01}\left(\Delta Z_{12} + 20\right) + \left(25r_{z01} - 25r_{x01} - t_{y01}\right) - \left(20 + r_1 + d_A\right) = 0 \quad (13)$$

$$\mathbf{SPH_1\text{-}S_4}: \left(\Delta X_{12} + 20\right) + r_{z04}\left(\Delta Y_{12} + 20\right) + r_{x04}\left(\Delta Z_{12} + 20\right) + \left(-25r_{x04} - 40r_{z04} - t_{y04}\right) - \left(20 + r_1 + d_B\right) = 0 \quad (14)$$

$$\mathbf{SPH_1\text{-}S_5}: -r_{z05}\left(\Delta X_{12} + 20\right) - r_{x05}\left(\Delta Y_{12} + 20\right) + \left(\Delta Z_{12} + 20\right) + \left(40r_{x05} + 25r_{z05} - t_{y05}\right) - \left(20 + r_1 + d_C\right) = 0 \quad (15)$$

Solving equations (13)÷(15) allows to calculate the assembly parameters of the first sphere in the box:

$$\Delta X_{12} = R_1 + d_B + r_1 - 20 \quad (16)$$

$$\Delta Y_{12} = R_1 + d_A + r_1 - 20 \tag{17}$$

$$\Delta Z_{12} = R_1 + d_c + r_1 - 20 \tag{18}$$

where d_i are the model parameters due to the form tolerance applied to the contact points of the spheres (where i = A, B, C, D, E, F and G with A, B, C, E and F are the contact points between the spheres and the box as shown in Figure 3).

The second sphere SPH_2 is assembled with the sub-assembly constituted by the box and SPH_1 through two spherical slider constrain joints, between SPH_2 and S_2 and between SPH_2 and S_5, and a spherical-spherical constrain joint between SPH_2 and SPH_1. The solution of the three constrain equations allows to calculate the assembly parameters of the second sphere on the sub-assembly constituted by the box and SPH_1.

The functional requirement g between SPH_2 and S_3 can be analytically evaluated by means of the formula for the calculation of the oriented distance between a plane and a sphere, that is:

$$g = n_x c_x + n_y c_y + n_z c_z - (R_2 + r_2 + d_G) \tag{19}$$

where n_x, n_y, n_z are the coefficients of the equation of the plane and c_x, c_y and c_z are the coordinates of the center of the sphere. The equations related to the three configurations and their solutions are reported in Appendix 1.

3. A point cloud variational model with operating conditions

Once generated, the two spheres were randomly rotated and they were assembled in the box, as described in the previous paragraph. Therefore, if the general position of each sphere is stable by considering the condition of balance among the applied forces was evaluated, that the applied forces are required to pass through the same point. The weight force is applied in the centre of gravity of the clouds (G_1 and G_2 in Figure 10a), the reactions are applied to the points of contact and they are directed to the centre of gravity of the sphere. The angles among these reactions and the normal vectors to the surfaces are β_1, β_2, β_3, β_4, β_5, β_6, as shown in Figure 10b. Those six angles should have a value smaller than the static friction limit angle in order to have a stable position of the sphere; for steel components they should be smaller than 2°. Otherwise, the sphere rotates until the values become smaller.

Then, the coordinates of the contact points among the components are identified and the corresponding form deviations are substituted in the equations (16)÷(18) for all configurations, in the equations (23)÷(25) for configuration 1, in the equations (30)÷(32) for configuration 2 and in the equations (37)÷(39) for configuration 3 respectively.

4. Numerical validation

To validate the new point cloud variational model with operating conditions, a pure geometrical approach has been developed too. Two spheres were simulated by means of eq. (1) to obtain two clouds of 235,822 points, which centre of gravity was calculated by the arithmetic mean of all the points coordinates. An absolute X-Y-Z reference system was placed as shown in Figure 8. The points of contact of the first sphere with the bottom (S_1), left (S_4) and back (S_5) sides of the box (A, B, C respectively in Figure 3) were identified as the more external points along the x, z and y axes and was brought into contact with the box in the identified points of contact. The points of contact of the second sphere with the sides of the box, for example with the right (S_2) and back (S_5) sides of the box (F and E in Figure 3) were defined as the more external points along the direction x and z axes .

The point of contact between the two spheres were identified by identifying the area surrounding the nominal point of contact, i.e. the point on which the spheres would touch if they were perfect, on each sphere since there the probability of contact is maximum. All couples of faced points in this area were identified, as those points having the same X and Z coordinates on the two contact zones. In particular, the couple of points that have the same X and at the minimum distance along the Z-axis for the configuration 1 were searched, the couple of points that have the same Z and at the minimum distance along the X-axis for the configuration 3. Finally, the couple of points nearest to the barycentre of two zones surrounding the nominal point of contact for the configuration 2. If the algorithm does not find a solution, the method increases the number of points around the nominal point of contact and the searching is repeated.

The points at minimum distance (called d_{min} in Figure 10a) were chosen as three points of contact between the two spheres. Therefore, all the points of the second sphere are shifted by the minimum

distance along Y-axis to bring the second sphere into contact with the first sphere just inserted in the box, as shown in Figure 10b.

Once assembled, the stability of the general position of each sphere was verified, as discussed in the paragraph 3. The distance between the upper side of the box and the point of the second sphere characterized by the maximum y coordinate was calculated as the value of the gap *g*.

5. Results comparison and discussion

10,000 runs were implemented in Monte Carlo simulation. Figure 11, Figure12 and Figure 13 show the results of the estimated gap *g* for the two models (model 1 is the variational model of the literature, model 2 is the new point cloud variational model with operating conditions) referring to the geometrical model (the reference model) in the three configurations. They detail the nominal value of the gap *g* (equal to 2.5834 mm for configuration 2 and equal to 1.2702 mm for the configuration 1 and 3), the range of ± 3σ around the mean value of the gap *g,* as estimated by the Monte Carlo simulations, and the tolerance range due to the worst case approach (classical approach in tolerance analysis). The two models give a distribution of the gap *g* completely contained inside the worst-case tolerance range.

Table 1 shows the results of the Anderson-Darling test to evaluate the normality of the obtained result distributions together with mean, standard deviation, Skewness and Kurtosis.

Model 1 (i.e. variational model of the literature) overestimates slightly the mean value of the *g* gap. It underestimates the standard deviation ($\frac{\sigma_1 - \sigma_{ref\,\mathrm{mod}}}{\sigma_{ref\,\mathrm{mod}}}$, where $\sigma_{ref\,\mathrm{mod}}$ is the standard deviation of the geometrical model) from about 6% to 23% depending on configuration. In fact, model 1 does not consider the correlation among the points of the spheres.

Model 2 (i.e. new point cloud variational model with operating conditions) is very close to the geometrical model in terms of both mean value and standard deviation.

To verify the homogeneity of variances, the Levene test was used for comparing the two models with the reference model in all three configuration of assembly, as shown in Figure 14. This test highlights the standard deviation of model 1 that is significantly different from that of geometrical model (the reference

model), as well as the standard deviation of the model 2.

The simulation times of model 2 is comparable with that of geometrical model (~110,000 s), but it is significantly higher than that of model 1 (few seconds). Therefore, model 1 is a good choice in terms of simulation time, if possible to accept an underestimation of gap *g*. Model 2 instead has a general structure that may be easily applicable to any kind of assemblies by requiring a short computational time, at the same time guaranteeing a good agreement with the reference geometrical model. The geometrical model requires to redo the modelling again, when the considered assembly changes; therefore, it cannot be easily implement in CAT software.

6. Conclusions

This work presents a new point-clouds variational model that takes into account both the manufacturing signature of the part surfaces and the operating conditions, such as gravity and friction that set in the assembly cycle.

The new variation model better reproduces the actual assembling of the machined spheres into a box, in presence of weight and friction forces, than the variational model of the literature. This aspect is evidenced by the mean value and the standard deviation of the new model that are not statistically different from those due to the reference model. The variational model of the literature seems to underestimate the tolerance range of the gap *g* of more than 6%, but it employs a simulation time of a few seconds.

The drawback of these models that involve the manufacturing signature and the operating conditions is the simulation times that must be reduced. It is currently matter of further study by evaluating the number of points needed to represent the skin model and the geometrical reasons to identify the contact points. The application of the new variational model to further different case studies is in progress, as well as an experimental activity to validate the calculation and analysis.

References

Ameta, G., Serge, S. & Giordano, M. 2011. Comparison of Spatial Math Models for Tolerance Analysis: Tolerance-Maps, Deviation Domain, and TTRS. *Journal of Computing and Information Science in Engineering,* 11**,** 021004-021004.

Anselmetti, B., Chavanne, R., Yang, J.-X. & Anwer, N. 2010. Quick GPS: A new CAT system for single-

part tolerancing. *Computer-Aided Design,* 42**,** 768-780.
Anwer, N., Schleich, B., Mathieu, L. & Wartzack, S. 2014. From solid modelling to skin model shapes: Shifting paradigms in computer-aided tolerancing. *CIRP Annals - Manufacturing Technology,* 63**,** 137-140.
Armillotta, A. & Semeraro, Q. 2013. Critical operating conditions for assemblies with parameter-dependent dimensions. *Proceedings of the Institution of Mechanical Engineers, Part B: Journal of Engineering Manufacture,* 227**,** 735-744.
Ascione, R., Polini, W. & Semeraro, Q. 2010. Process Signature Modeling for Tolerance Analysis. *Journal of Computing and Information Science in Engineering,* 10**,** 021006.
Bo, C., Yang, Z., Wang, L. & Chen, H. 2013. A comparison of tolerance analysis models for assembly. *The International Journal of Advanced Manufacturing Technology,* 68**,** 739-754.
Boyer, M. & Stewart, N. F. 1991. Modeling Spaces for Toleranced Objects. *The International Journal of Robotics Research,* 10**,** 570-582.
Chen, H., Jin, S., Li, Z. & Lai, X. 2014. A comprehensive study of three dimensional tolerance analysis methods. *Computer-Aided Design,* 53**,** 1-13.
Corrado, A., Polini, W., Moroni, G. & Petrò, S. 2016. 3D Tolerance Analysis with Manufacturing Signature and Operating Conditions. *Procedia CIRP,* 43**,** 130-135.
Cressie, N. 2015. *Statistics for spatial data*, John Wiley & Sons.
Gupta, S. & Turner, J. U. 1993. Variational solid modeling for tolerance analysis. *IEEE Computer Graphics and Applications,* 13**,** 64-74.
Martino, P. M. & Gabriele, G. A. 1989. Application of Variational Geometry to the Analysis of Mechanical Toleranced. *Conference on Failure Prevention and Reliability ASME Paper,* 16**,** 19-27.
Marziale, M. & Polini, W. Tolerance Analysis: A New Model Based on Variational Solid Modelling. ASME 2010 10th Biennial Conference on Engineering Systems Design and Analysis, 2010. American Society of Mechanical Engineers, 383-392.
Moroni, G. & Polini, W. 2003. Tolerance-based Variations in Solid Modeling. *Journal of Computing and Information Science in Engineering,* 3**,** 345-352.
Paetzold, K., Wittmann, S., Stoll, T. & Helwig, S. Registration of measured and simulated non-ideal geometry using optimization methods. *In:* WECKENMANN, A., ed. International Seminar on Computet Aided Tolerancing (10th CIRP International Seminar on Computet Aided Tolerancing), 2007 Erlangen.
Polini, W. 2011. Geometric Tolerance Analysis. *In:* COLOSIMO, B. M. & SENIN, N. (eds.) *Geometric Tolerances: Impact on Product Design, Quality Inspection and Statistical Process Monitoring.* London: Springer London.
Polini, W. 2012. Taxonomy of models for tolerance analysis in assembling. *International Journal of Production Research,* 50**,** 2014-2029.
Samper, S., Adragna, P.-A., Favreliere, H. & Pillet, M. 2009. Modeling of 2D and 3D Assemblies Taking Into Account Form Errors of Plane Surfaces. *Journal of Computing and Information Science in Engineering,* 9**,** 041005-041005-12.
Schleich, B., Anwer, N., Mathieu, L. & Wartzack, S. 2014. Skin Model Shapes: A new paradigm shift for geometric variations modelling in mechanical engineering. *Computer-Aided Design,* 50**,** 1-15.
Stoll, T., Wittmann, S. & Meerkamm, H. 2010. Tolerance analysis with detailed part modeling. *Product Lifecycle Management: Geometric Variations***,** 231-243.
Weihua, N. & Zhenqiang, Y. 2013. Integrating cylindricity error into tolerance analysis of precision rotary assemblies using Jacobian–Torsor model. *Proceedings of the Institution of Mechanical Engineers, Part C: Journal of Mechanical Engineering Science,* 227**,** 2517-2530.

Appendix 1

Configuration 1

The three constrain equations of the second sphere SPH_2 on the sub-assembly constituted by the box and SPH_1 are:

SPH_2-S_2: $-\left(\Delta X_{13}+30\right)-r_{z02}\left(\Delta Y_{13}+58.73\right)+r_{x02}\left(\Delta Z_{13}+20\right)+\left(50+40r_{z02}-R_2-r_2-d_F-25r_{x02}-t_{y02}\right)=0$ (20)

SPH_2-S_5: $-r_{z05}\left(\Delta X_{13}+30\right)-r_{x05}\left(\Delta Y_{13}+58.73\right)+\left(\Delta Z_{13}+20\right)+\left(50+40r_{x05}-R_2-r_2-d_E+25r_{z05}-t_{y05}\right)=0$ (21)

SPH_2-SPH_1: $\left(\Delta X_{13}-\Delta X_{12}+10\right)^2+\left(\Delta Y_{13}-\Delta Y_{12}+38.73\right)^2+\left(\Delta Z_{13}-\Delta Z_{12}\right)^2-\left(R_1+R_2+r_1+r_2+d_{D1}+d_{D2}\right)^2=0$ (22)

The solution of equations (19)÷(21) allows to calculate the assembly parameters of the second sphere on the sub-assembly constituted by the box and SPH_1:

$$\Delta X_{13}=20-d_F-r_2-R_2 \tag{23}$$

$$\begin{aligned}\Delta Y_{13}=&R_1+d_A+r_1+\left(100R_1+20R_2+60d_B+40d_C-40d_E+60d_F+100r_1+20r_2+2R_1R_2-2R_1d_B-2R_1d_C+2R_1d_{D1}+\right.\\&+2R_1d_{D2}+2R_2d_{D1}+2R_2d_{D2}-2R_1r_1+2R_1r_2+2R_2r_1+2R_2r_2+2d_{D1}d_{D2}-2d_Br_1-2d_Cr_1+2d_{D1}r_1+2d_{D2}r_1+\\&+2d_{D1}r_2+2d_{D2}r_2+2R_1\Delta z_{12}-2R_1\left(-\Delta X_{12}\right)+2r_1r_2-d_B\left(-2\Delta X_{12}\right)+d_C\left(2\Delta Z_{12}\right)+r_1\left(2\Delta Z_{12}\right)-r_1\left(-2\Delta X_{12}\right)+\\&\left.-R_1^2+R_2^2-d_B^2-d_C^2+d_{D1}^2+d_{D2}^2-r_1^2+r_2^2-\left(\Delta Z_{12}\right)^2-\left(\Delta X_{12}\right)^2-1700\right)^{0.5}-5873/100\end{aligned} \tag{24}$$

$$\Delta Z_{13}=R_2+d_E+r_2-20 \tag{25}$$

The functional requirement *g* between SPH_2 and S_3 can be analytically evaluated by means of the formula (19). By substituting the model parameters of the plane and the sphere, it is possible to obtain the following equation:

$$g=1.27+20-\Delta Y_{13}-R_2-r_2-d_G \tag{26}$$

Configuration 2

In this case the three constrain equations are:

SPH_2-S_2: $-\left(\Delta X_{13}+30\right)-r_{z02}\left(\Delta Y_{13}+57.42\right)+r_{x02}\left(\Delta Z_{13}+30\right)+\left(50-t_{y02}+40r_{z02}-R_2-r_2-d_F-25r_{x02}\right)=0$ (27)

SPH_2-S_6: $-r_{z06}\left(\Delta X_{13}+30\right)+r_{x06}\left(\Delta Y_{13}+57.42\right)-\left(\Delta Z_{13}+30\right)-\left(40r_{x06}+R_2+r_2+d_E-25r_{z05}+t_{y06}\right)=0$ (28)

SPH_2-SPH_1: $\left(\Delta X_{13}-\Delta X_{12}+10\right)^2+\left(\Delta Y_{13}-\Delta Y_{12}+37.42\right)^2+\left(\Delta Z_{13}-\Delta Z_{12}+10\right)^2-\left(R_1+R_2+r_1+r_2+d_{D1}+d_{D2}\right)^2=0$ (29)

Solving equations (27)÷(29) allows to define the assembly parameters of the second sphere on the sub-

assembly constituted by the box and SPH_1:

$$\Delta X_{13} = 20 - d_F - r_2 - R_2 \tag{30}$$

$$\begin{aligned}\Delta Y_{13} = {} & R_1 + d_A + r_1 + \left(120R_1 + 120R_2 + 60d_B + 60d_C + 60d_E + 60d_F + 120r_1 + 120r_2 + 2R_1R_2 - 2R_1d_B - 2R_1d_C + 2R_1d_{D1} + \right. \\ & + 2R_1d_{D2} + 2R_2d_{D1} + 2R_2d_{D2} - 2R_1r_1 + 2R_1r_2 + 2R_2r_1 + 2R_2r_2 + 2d_{D1}d_{D2} - 2d_Br_1 - 2d_Cr_1 + 2d_{D1}r_1 + 2d_{D2}r_1 + \\ & + 2d_{D1}r_2 + 2d_{D2}r_2 + 2R_1\Delta z_{13} - 2R_1\left(-\Delta X_{13}\right) + 2r_1r_2 - d_B\left(-2\Delta X_{13}\right) + d_C\left(2\Delta Z_{13}\right) + r_1\left(2\Delta Z_{13}\right) - r_1\left(-2\Delta X_{13}\right) + \\ & \left. - R_1^2 + R_2^2 - d_B^2 - d_C^2 + d_{D1}^2 + d_{D2}^2 - r_1^2 + r_2^2 - \left(-\Delta Z_{13}\right)^2 - \left(-\Delta X_{13}\right)^2 - 4200\right)^{0.5} - 2871/50\end{aligned} \tag{31}$$

$$\Delta Z_{13} = -R_2 - d_E - r_2 + 20 \tag{32}$$

The functional requirement *g* between SPH_2 and S_3 can be analytically evaluated by means of the formula for the calculation of the minimum oriented distance between a plane and a sphere, whereas the model parameters of the plane and the sphere are inserted in the equation:

$$g = 2.58 + 20 - \Delta Y_{13} - R_2 - r_2 - d_G \tag{33}$$

Configuration 3

The three constrain equations are:

SPH_2-S_4: $\left(\Delta X_{13} + 20\right) + r_{z04}\left(\Delta Y_{13} + 58.73\right) + r_{x04}\left(\Delta Z_{13} + 30\right) + \left(-40r_{z04} - R_2 - r_2 - d_F - 25r_{x04} - t_{y04}\right) = 0$ (34)

SPH_2-S_6: $-r_{z06}\left(\Delta X_{13} + 20\right) + r_{x06}\left(\Delta Y_{13} + 58.73\right) - \left(\Delta Z_{13} + 30\right) - \left(40r_{x06} + R_2 + r_2 + d_E - 25r_{z06} + t_{y06}\right) = 0$ (35)

SPH_2-SPH_1: $\left(\Delta X_{13} - \Delta X_{12}\right)^2 + \left(\Delta Y_{13} - \Delta Y_{12} + 38.73\right)^2 + \left(\Delta Z_{13} - \Delta Z_{12} + 10\right)^2 - \left(R_1 + R_2 + r_1 + r_2 + d_{D1} + d_{D2}\right)^2 = 0$ (36)

The solution of equations (34)÷(36) allows the calculation of the assembly parameters of the second sphere on the sub-assembly constituted by the box and SPH_1:

$$\Delta X_{13} = -20 + d_F + r_2 + R_2 \tag{37}$$

$$\begin{aligned}\Delta Y_{13} = {} & R_1 + d_A + r_1 + \left(100R_1 + 20R_2 + 40d_B + 60d_C + 60d_E - 40d_F + 100r_1 + 20r_2 + 2R_1R_2 - 2R_1d_B - 2R_1d_C + 2R_1d_{D1} + \right. \\ & + 2R_1d_{D2} + 2R_2d_{D1} + 2R_2d_{D2} - 2R_1r_1 + 2R_1r_2 + 2R_2r_1 + 2R_2r_2 + 2d_{D1}d_{D2} - 2d_Br_1 - 2d_Cr_1 + 2d_{D1}r_1 + 2d_{D2}r_1 + \\ & + 2d_{D1}r_2 + 2d_{D2}r_2 + 2R_1\Delta z_{13} + 2R_1\left(\Delta X_{13}\right) + 2r_1r_2 + d_B\left(2\Delta X_{13}\right) - d_C\left(-2\Delta Z_{13}\right) + r_1\left(2\Delta Z_{13}\right) + r_1\left(2\Delta X_{13}\right) + \\ & \left. - R_1^2 + R_2^2 - d_B^2 - d_C^2 + d_{D1}^2 + d_{D2}^2 - r_1^2 + r_2^2 - \left(-\Delta Z_{12}\right)^2 - \left(-\Delta X_{12}\right)^2 - 1700\right)^{0.5} - 5.873/100\end{aligned} \tag{38}$$

$$\Delta Z_{13} = -R_2 - d_E - r_2 + 20 \tag{39}$$

The functional requirement *g* between SPH_2 and S_3 may be evaluated by means of the analytical equation:

$$g = 1.27 + 20 - \Delta Y_{13} - R_2 - r_2 - d_G \tag{40}$$

Figure captions

Figure 1 - Case study

Figure 2 - Point cloud of a SAR(1) (dimension in mm, amplified 100 times)

Figure 3 - Case study: The three considered configurations of the case study

Figure 4 - Configuration 1

Figure 5 - Configuration 2

Figure 6 - Configuration 3

Figure 7 - Scheme of the new point cloud variational model with operating conditions

Figure 8 - Datum reference frames assigned to the case study

Figure 9 - Assembly graphs: a) Configuration 1, b) Configuration 2, c) Configuration 3

Figure 10 - a) Minimum distance between the two spherical clouds, b) β_i angles to evaluate if each spherical cloud is stable (amplified 100 times)

Figure 11 - Results of configuration 1

Figure 12 - Results of configuration 2

Figure 13 - Results of configuration 3

Figure 14 - Levene's test results: a) Configuration 1, b) Configuration 2, c) Configuration 3

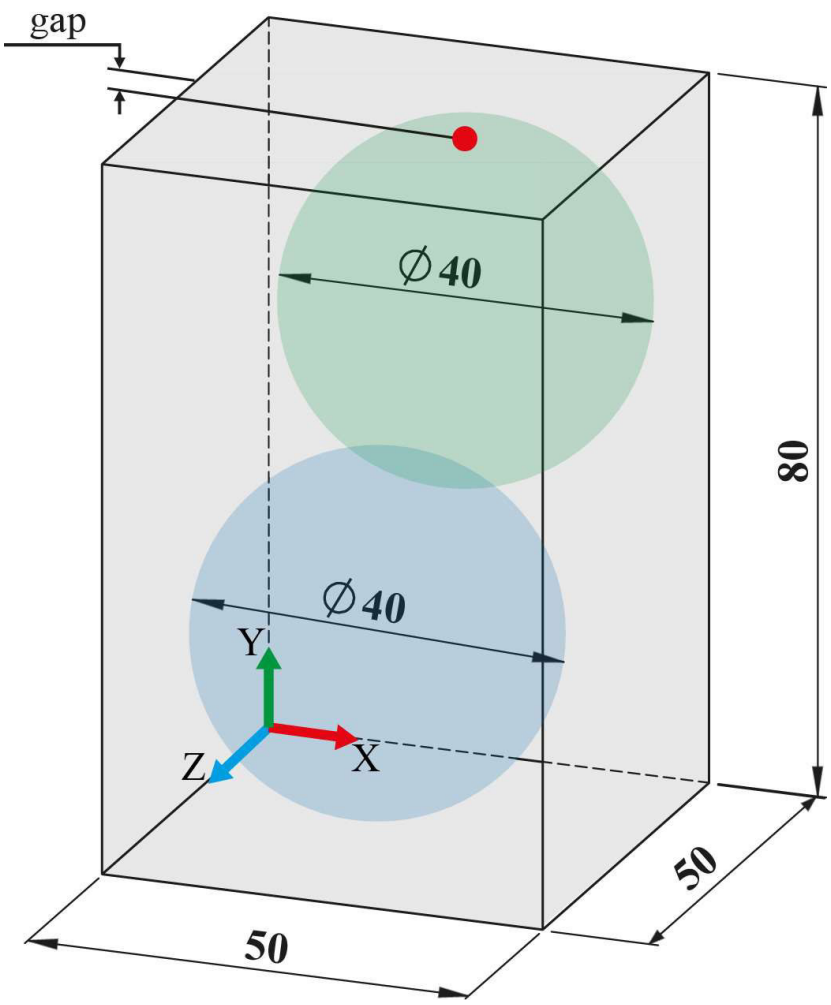

Figure 1 - Case study

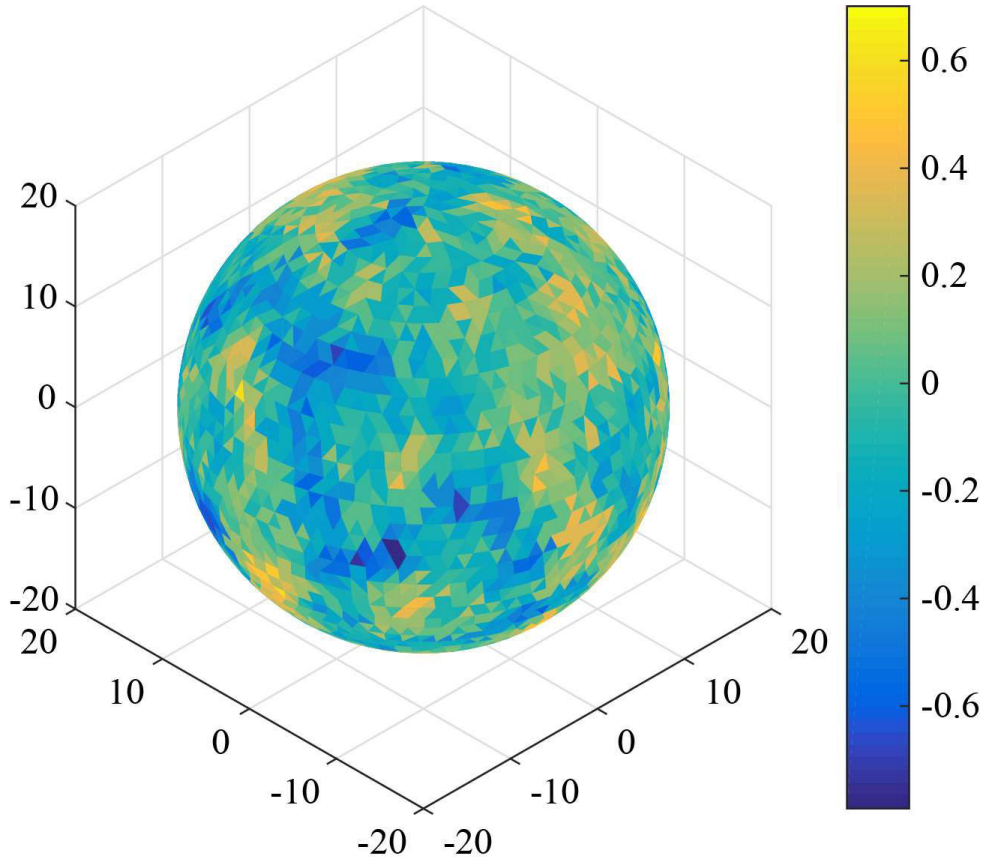

Figure 2 - Point cloud of a SAR(1) (dimension in mm, amplified 100 times)

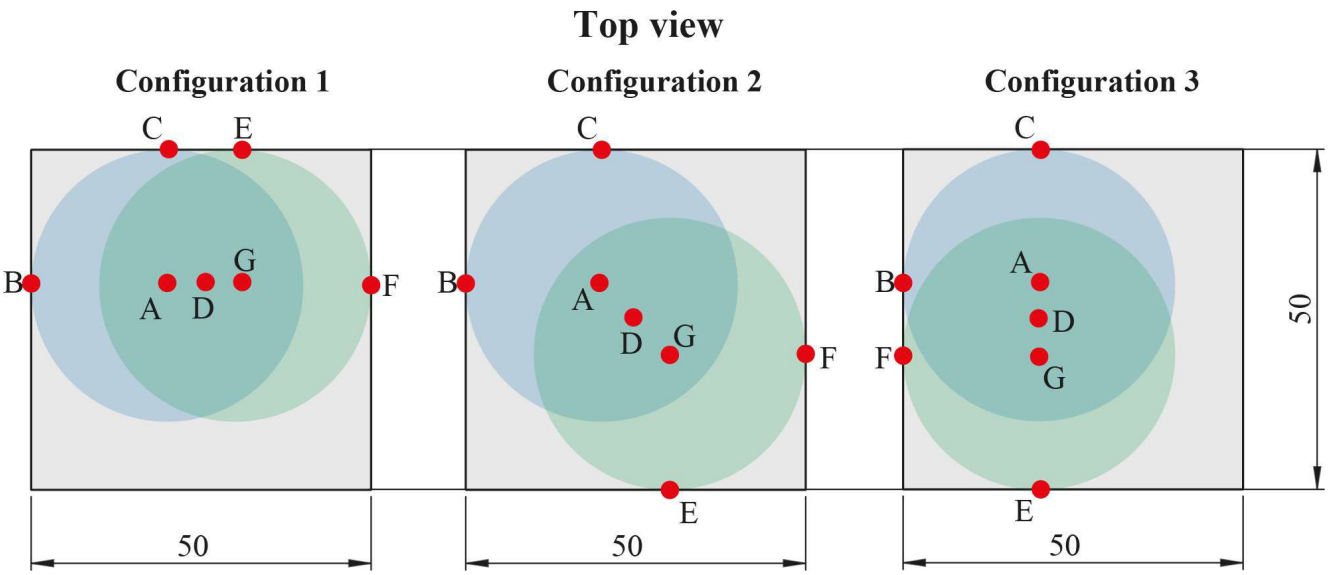

Figure 3 - Case study: The three considered configurations of the case study

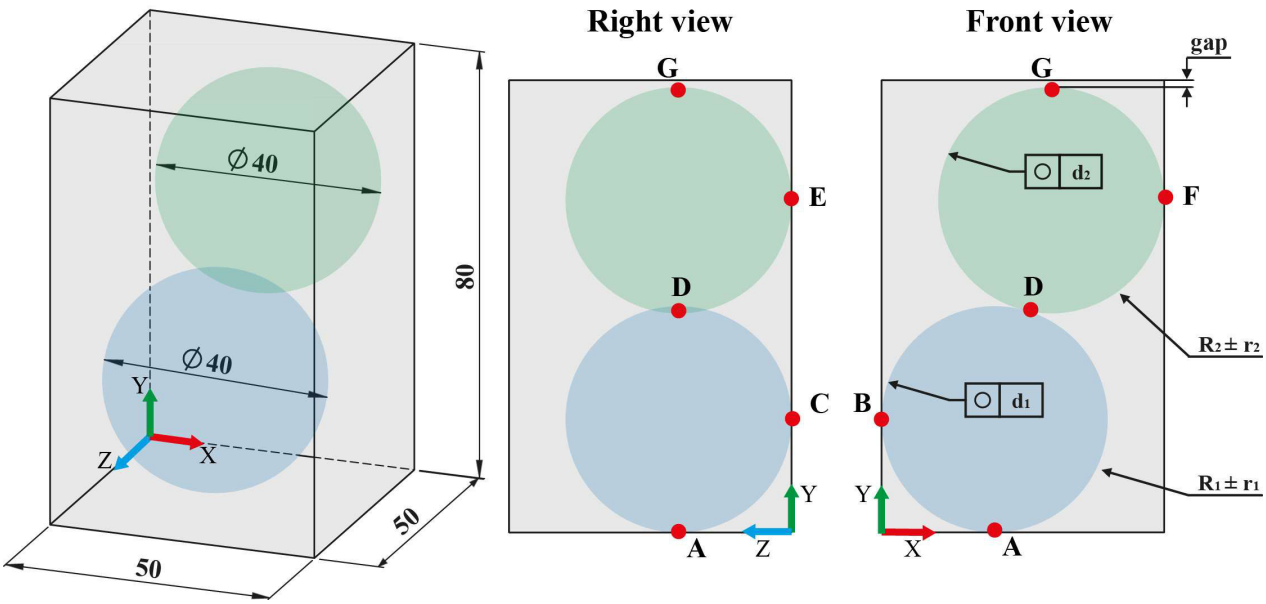

Figure 4 - Configuration 1

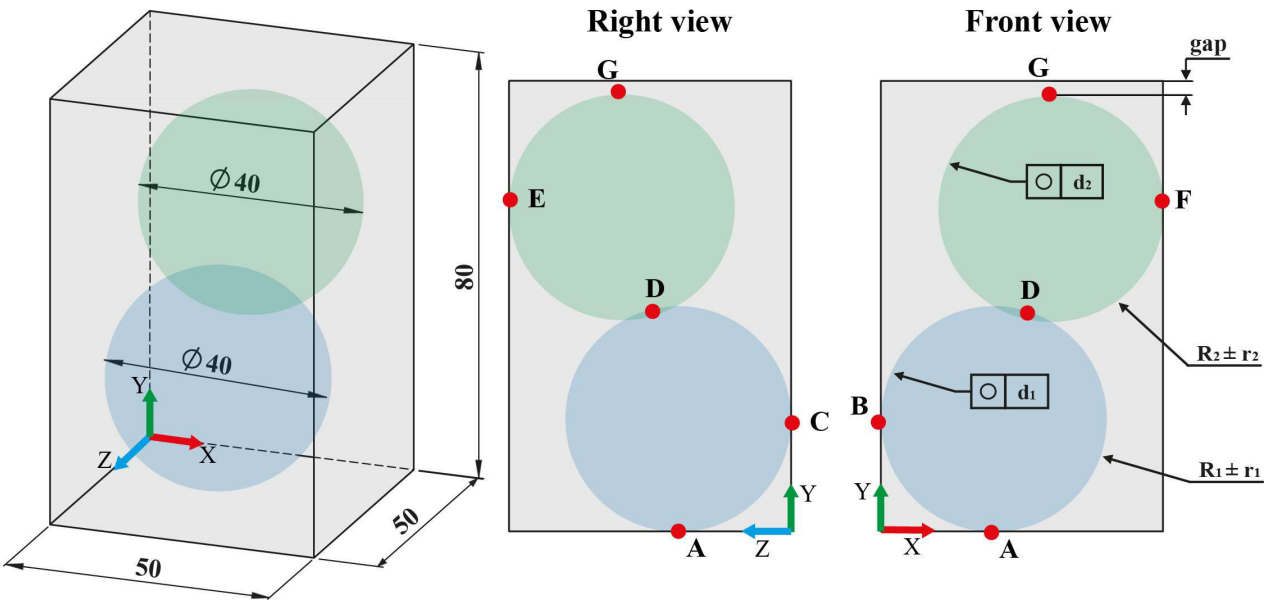

Figure 5 - Configuration 2

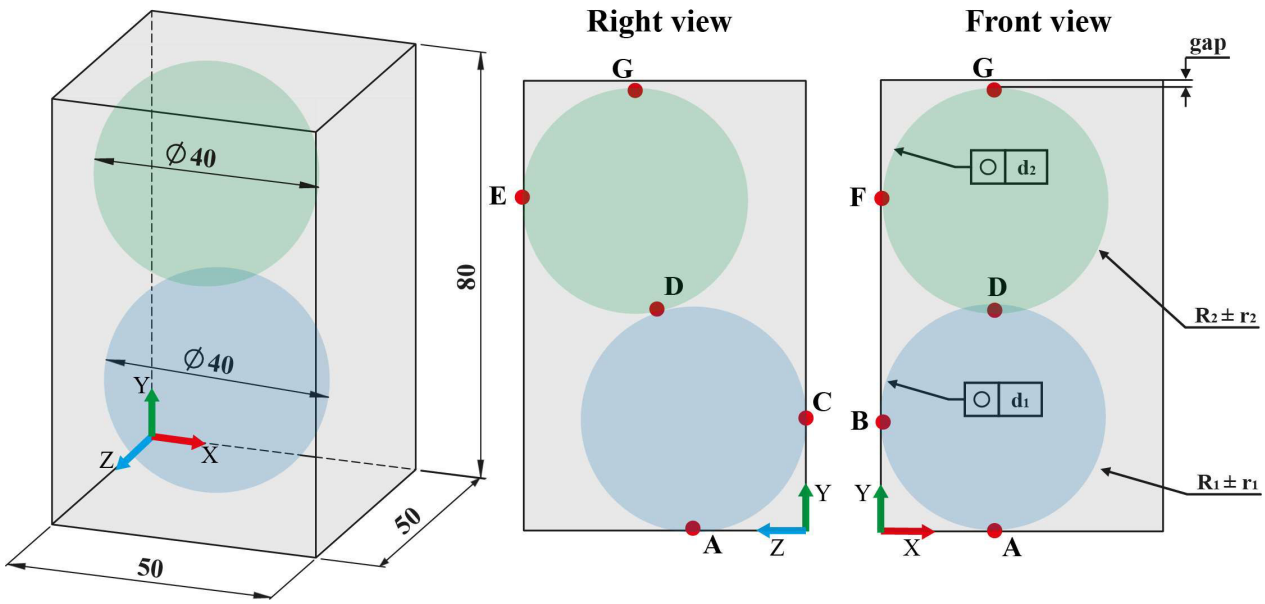

Figure 6 - Configuration 3

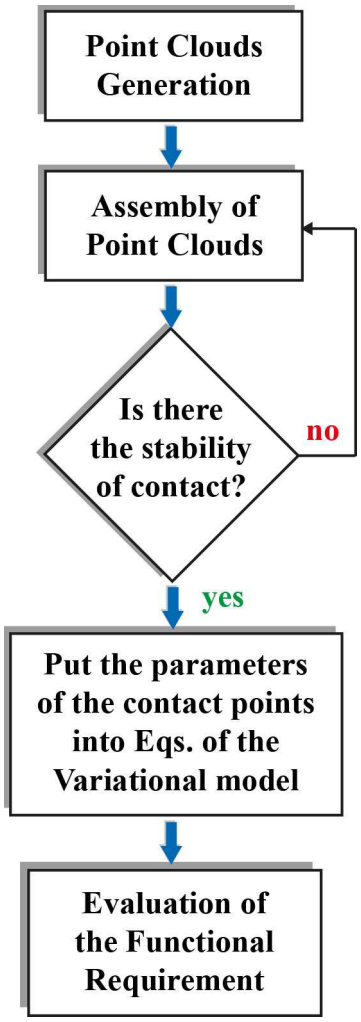

Figure 7 - Scheme of the new point cloud variational model with operating conditions

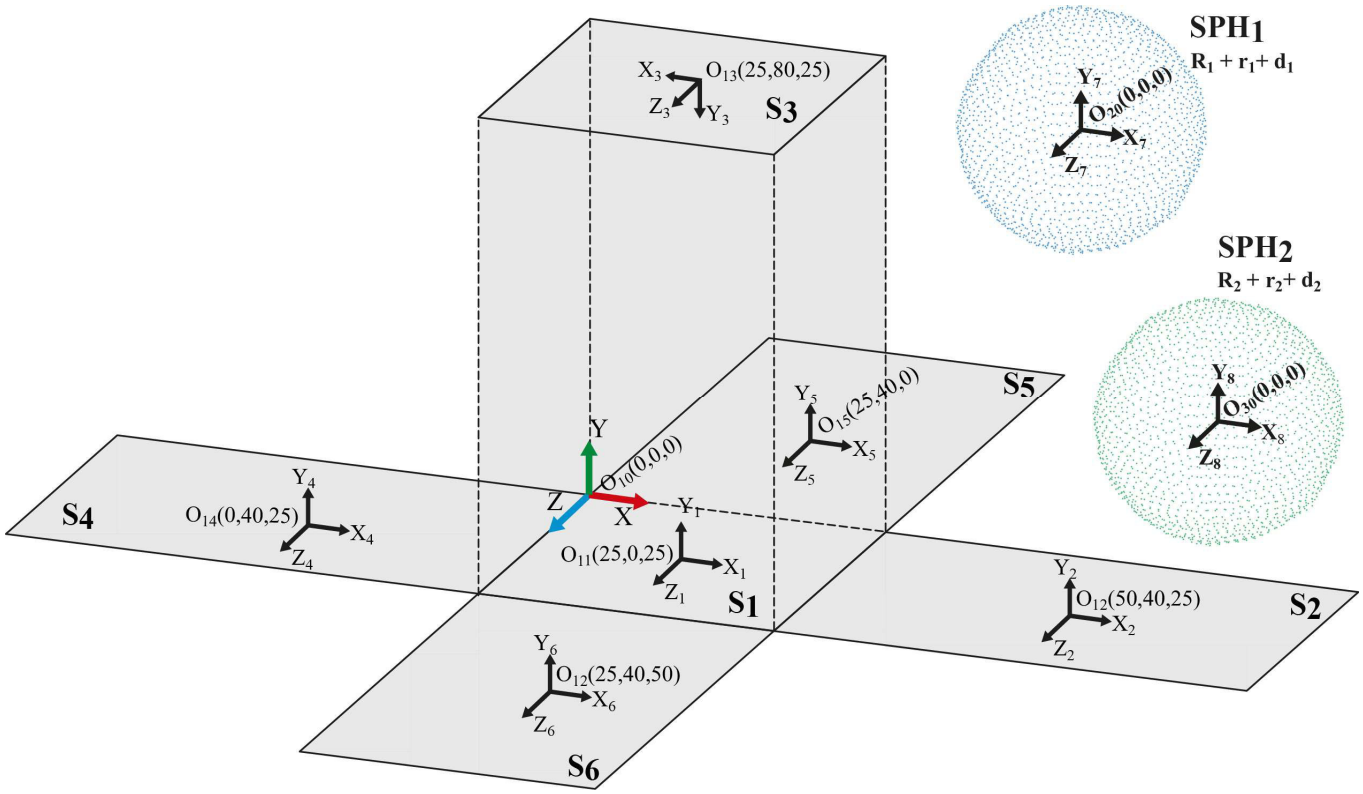

Figure 8 - Datum reference frames assigned to the case study

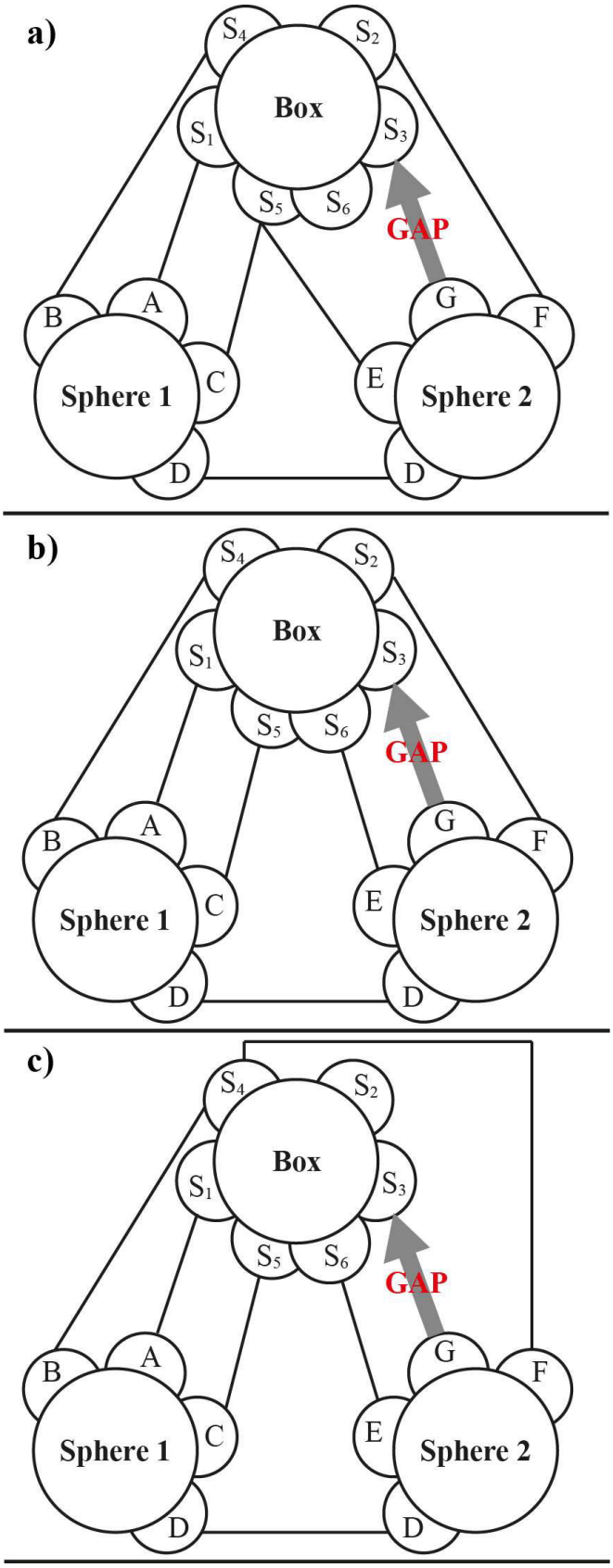

Figure 9 - Assembly graphs: a) Configuration 1, b) Configuration 2, c) Configuration 3

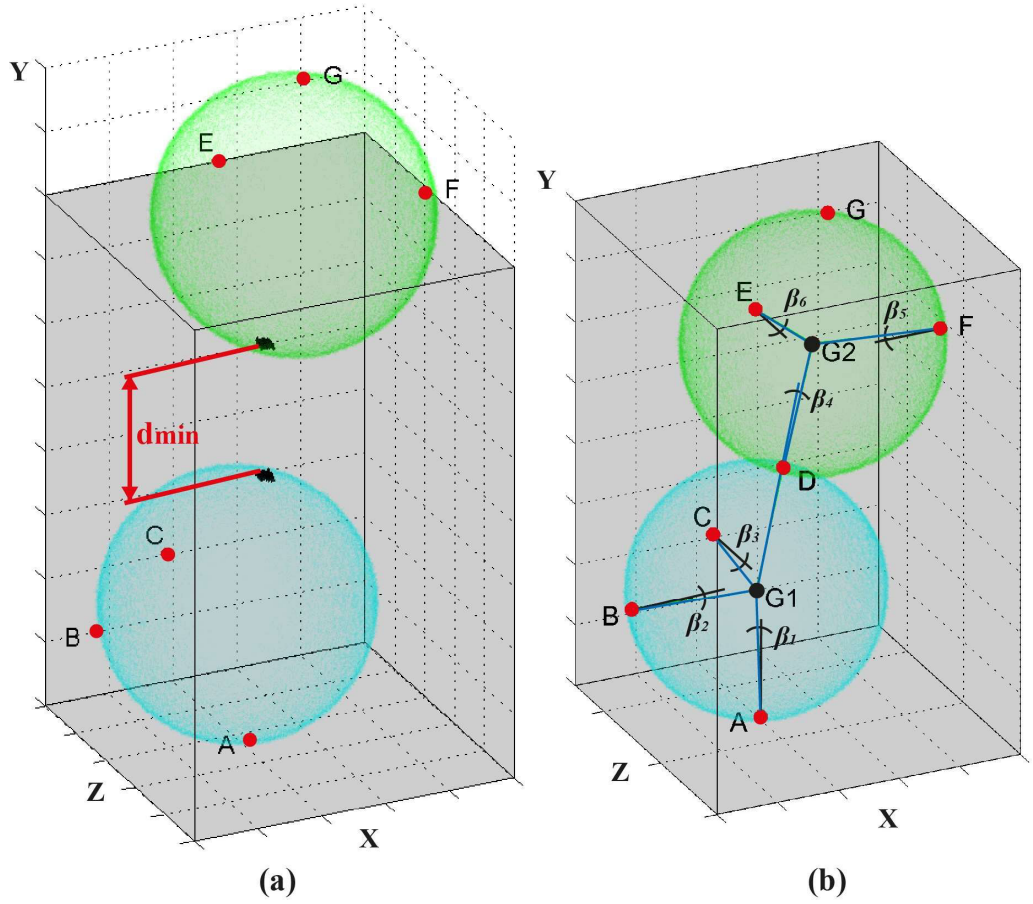

Figure 10 - a) Minimum distance between the two spherical clouds, b) βi angles to evaluate if each spherical cloud is stable (amplified 100 times)

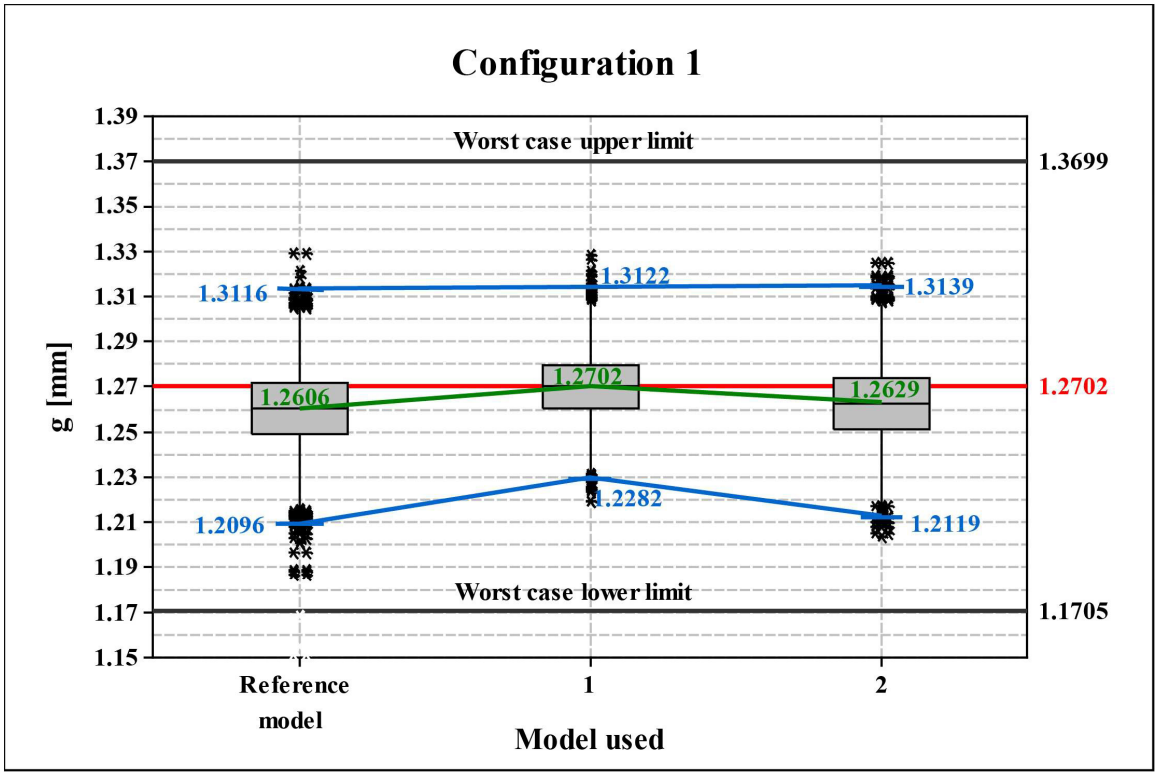

Figure 11 - Results of configuration 1

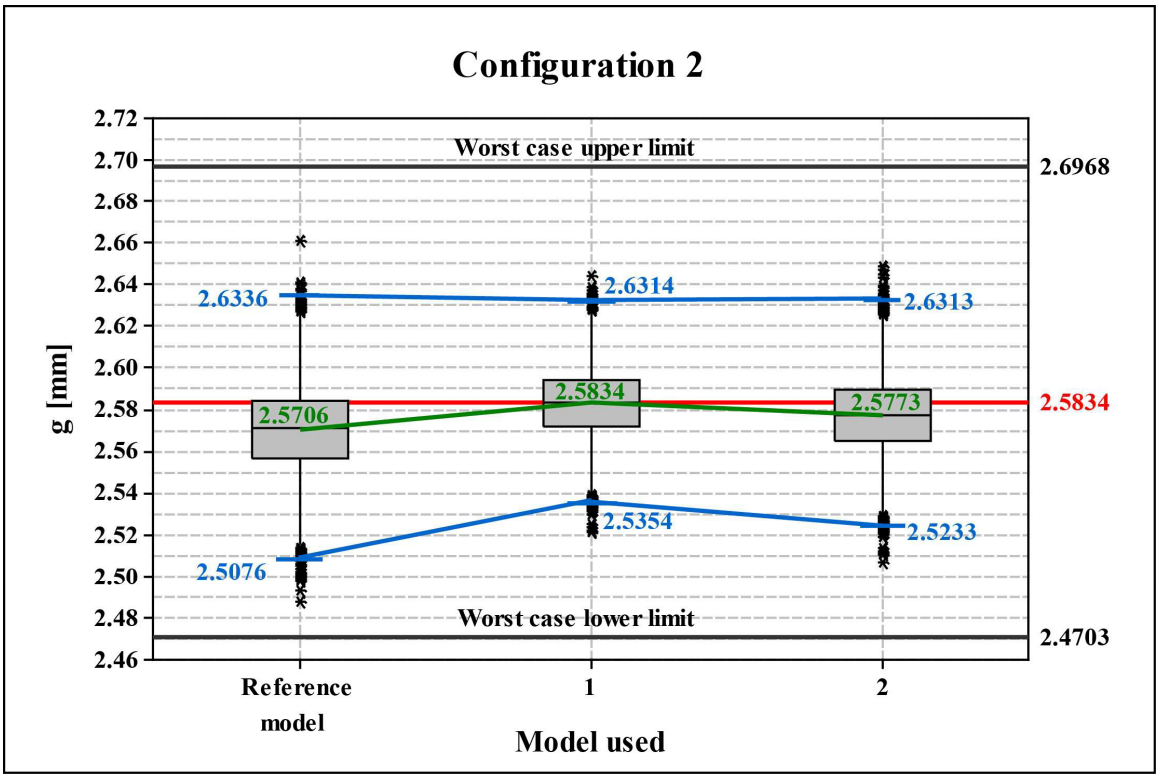

Figure 12 - Results of configuration 2

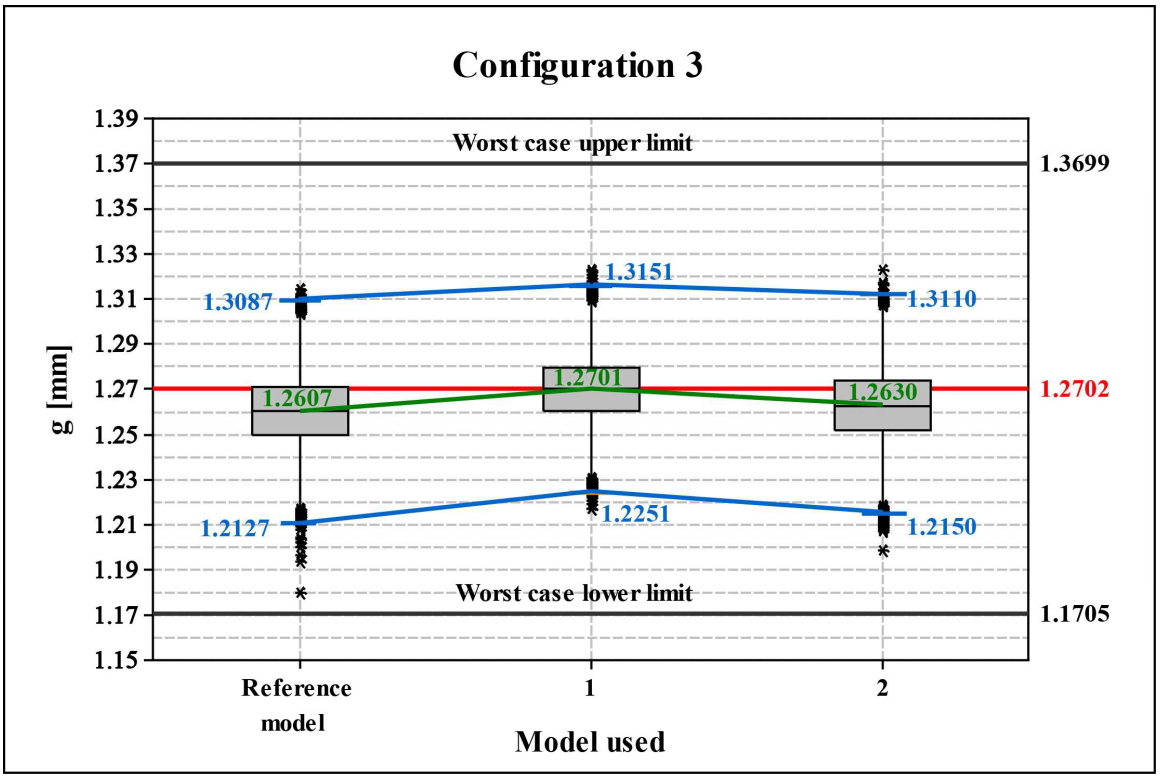

Figure 13 - Results of configuration 3

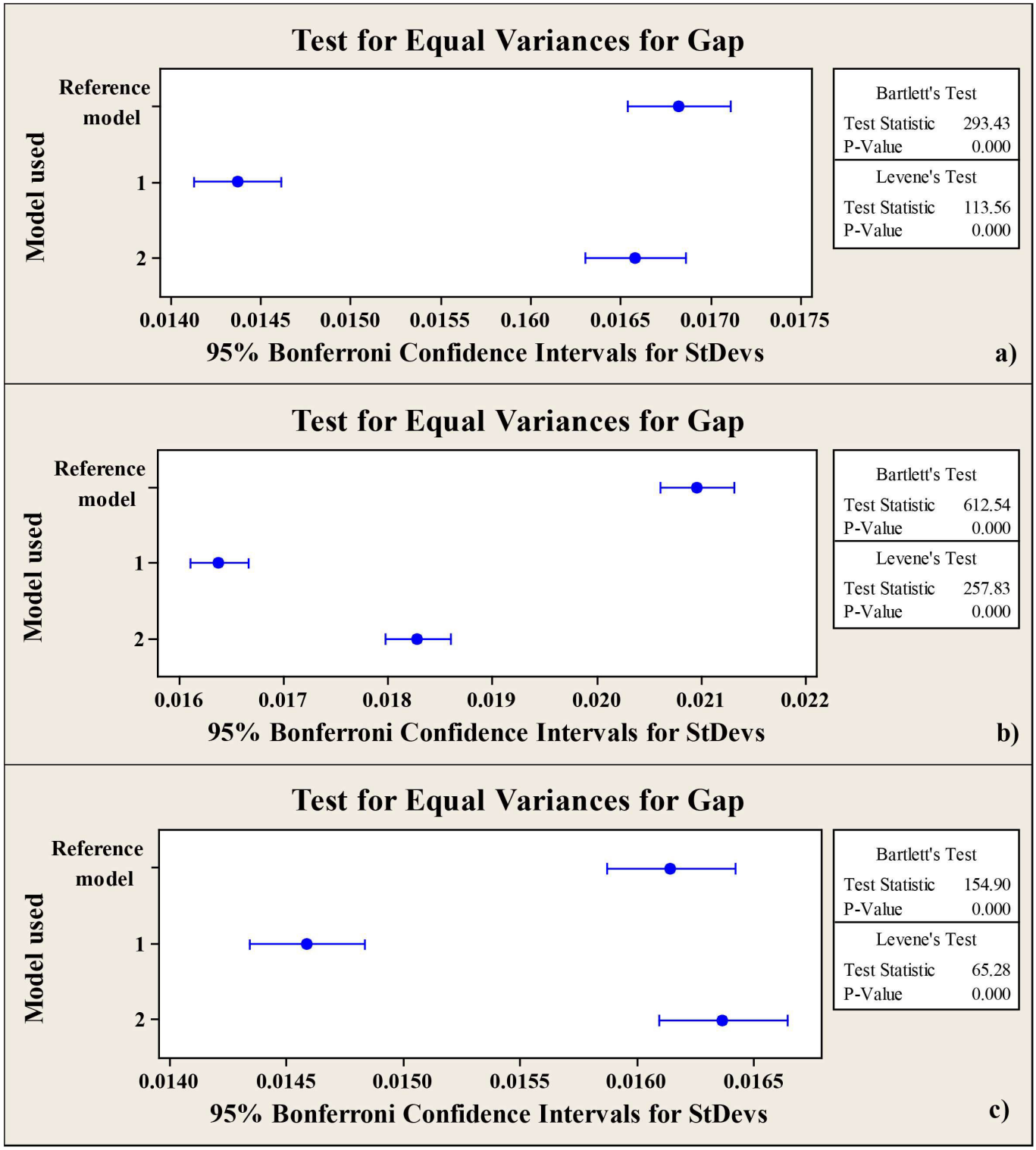

Figure 14 - Levene's test results: a) Configuration 1, b) Configuration 2, c) Configuration 3

Table captions

Table 1 - Simulation results (10,000 runs)

Table 1 - Simulation results (10,000 runs)

Configuration	Model	Mean [mm]	σ [mm]	A-Squared	P-value	Skew.	Kurt.
	Reference	1.2606	0.017	2.28	<0.005	-0.254	1.557
1	1	1.2702	0.014	0.43	0.309	0.017	-0.001
	2	1.2629	0.017	0.23	0.798	0.013	0.014
	Reference	2.5706	0.021	0.60	0.120	-0.051	0.034
2	1	2.5834	0.016	0.32	0.535	-0.018	0.013
	2	2.5773	0.018	0.43	0.301	-0.026	0.091
	Reference	1.2607	0.016	0.52	0.188	-0.011	0.045
3	1	1.2701	0.015	0.37	0.425	-0.021	-0.042
	2	1.2630	0.016	0.56	0.149	0.013	-0.012